Rho Kinase Differentially Regulates Phosphorylation of Nonmuscle Myosin II Isoforms A and B during Cell Rounding and Migration*[s]

Joshua C. Sandquist[‡1], Katherine I. Swenson[‡], Kris A. DeMali[§2], Keith Burridge[§], and Anthony R. Means[‡3]

From the ‡Department of Pharmacology and Cancer Biology, Duke University Medical Center, Durham, North Carolina 27710 and §Department of Cell and Developmental Biology and Lineberger Comprehensive Cancer Center, University of North Carolina, Chapel Hill, North Carolina 27599

The actin-myosin cytoskeleton is generally accepted to produce the contractile forces necessary for cellular processes such as cell rounding and migration. All vertebrates examined to date are known to express at least two isoforms of non-muscle myosin II, referred to as myosin IIA and myosin IIB. Studies of myosin IIA and IIB in cultured cells and null mice suggest that these isoforms perform distinct functions. However, how each myosin II isoform contributes individually to all the cellular functions attributed to "myosin II" has yet to be fully characterized. Using isoform-specific small-interfering RNAs, we found that depletion of either isoform resulted in opposing migration phenotypes, with myosin IIA- and IIB-depleted cells exhibiting higher and lower wound healing migration rates, respectively. In addition, myosin IIA-depleted cells demonstrated impaired thrombin-induced cell rounding and undertook a more motile morphology, exhibiting decreased amounts of stress fibers and focal adhesions, with concomitant increases in cellular protrusions. Cells depleted of myosin IIB, however, were efficient in thrombin-induced cell rounding, displayed a more retractile phenotype, and maintained focal adhesions but only in the periphery. Last, we present evidence that Rho kinase preferentially regulates phosphorylation of the regulatory light chain associated with myosin IIA. Our data suggest that the myosin IIA and IIB isoforms are regulated by different signaling pathways to perform distinct cellular activities and that myosin IIA is preferentially required for Rho-mediated contractile functions.

Nonmuscle myosin II (henceforth, myosin II) is a ubiquitous molecular motor that binds and contracts filamentous actin (F-actin) in an ATP-dependent manner (1, 2). The forces that are generated by contraction of the actin-myosin cytoskeleton contribute to a diverse array of cellular processes in a variety of cell types, including cytokinesis (3), platelet activation (4), cell rounding (5), and cell migration (6, 7). The latter is a highly complex process in which cells can participate either as isolated individuals, such as neuroblast migration during development or tumor cell metastasis, or as groups, as exemplified by the coordinated movement of epithelial sheets during dorsal closure or wound healing.

The process of cell migration is often described as a cycle of coordinated steps (8, 9) in which the first step is protrusion of the membrane in the intended direction of movement followed by stabilization of the extended membrane via the formation of new adhesion sites. Last, the cell undergoes contraction, in which the cell body translocates forward accompanied by tail detachment and retraction. Although myosin II is thought to perform multiple functions during the migration cycle, one aspect of cell migration for which a clear requirement for myosin II-based contractility has been demonstrated is the regulation of focal adhesions. Focal adhesions are integrin-based, large multimolecular assemblies that form a structural bridge between the substrate and the actin cytoskeleton (10). Efficient migration requires the proper coordination of adhesion assembly in the front and de-adhesion in the rear (11), and myosin II shares an intimate relationship with focal adhesions as their assembly, maturation, and dynamics (12–14) depend on myosin II-induced tension.

Much of the work describing the importance of myosin II in cell motility has been performed using the genetically tractable model systems *Dictyostelium* (7, 15) and *Drosophila* (16–18). It is important to note, however, that *Drosophila* and *Dictyostelium* harbor only a single myosin II molecule, whereas vertebrates are known to express three distinct myosin IIs, referred to as myosin IIA, IIB, and IIC (1, 19, 20). Myosin II is a hexameric molecule comprised of a pair of heavy chains, a pair of essential light chains, and a pair of regulatory light chains (RLCs)[4] (2). The distinction between the three myosin II molecules is based upon their unique heavy chain isoforms. Interestingly, each isoform performs the same basic molecular function, which is the binding and contraction of F-actin in an ATP-dependent manner, and the activities of all three are

[1] A Howard Hughes Medical Institute Predoctoral Fellow.
[2] Present address: Dept. of Biochemistry, University of Iowa, Iowa City, IA 52242.
[3] To whom correspondence should be addressed: Dept. of Pharmacology and Cancer Biology, Duke University Medical Center, P. O. Box 3813, Durham, NC 27702-3813. Tel.: 919-681-6209; Fax: 919-681-7767; E-mail: means001@mc.duke.edu.

[4] The abbreviations used are: RLC, myosin regulatory light chain; IIA, nonmuscle myosin IIA; IIB, nonmuscle myosin IIB; IIC, nonmuscle myosin IIC; siRNA, small-interfering RNA; ROCK, Rho kinase.

thought to be regulated in a similar fashion; that is, through phosphorylation of the RLC (2). Thus, how each myosin II isoform performs different cellular functions *in vivo* is not understood. In this study we identified distinct functions of myosin IIA and IIB (hereafter IIA and IIB, respectively) in epithelial cell sheet migration and thrombin-induced cell rounding. Our data demonstrate that these isoforms are differentially required for cell rounding, and each isoform uniquely contributes to the proper regulation of protrusions and adhesions and, thus, proper migration. Furthermore, we demonstrate that phosphorylation of the RLC associated with IIA or IIB is differentially regulated by Rho kinase, suggesting that at least part of how IIA and IIB perform discrete cellular functions is via selective regulation downstream from different signaling pathways.

EXPERIMENTAL PROCEDURES

Antibodies and Reagents—Monoclonal anti-vinculin (VIN-11-5, #V-4505) and monoclonal anti-β-actin (AC-15, #A-5441) were purchased from Sigma-Aldrich. Polyclonal myosin light chain 2 (#3672), polyclonal phospho-myosin light chain 2 (Ser-19, #3671), and polyclonal phospho-myosin light chain 2 (Thr-18/Ser-19) antibodies were purchased from Cell Signaling Technology. Polyclonal nonmuscle myosin II heavy chain A (#PRB-440P) and polyclonal nonmuscle myosin II heavy chain B (#PRB-445P) were purchased from Covance Research Products. Fluorescein-conjugated AffiniPure goat anti-mouse IgG (#115-095-146) and Cy3-conjugated AffiniPure goat anti-rabbit IgG (#111-166-003) were purchased from Jackson ImmunoResearch Laboratories, Inc. Rhodamine-conjugated phalloidin was from Molecular Probes (#R415), and Y-27632 was from Calbiochem (#688000).

Cell Line and Culture Conditions—The cell lines used in this study were the epithelial-derived, lung carcinoma A549 cell line and the epithelial-derived, breast adenocarcinoma MDA-MB-231 cell line. Both lines were maintained in Dulbecco's modified Eagle's medium supplemented with 10% fetal bovine serum (heat-inactivated for A549) and antibiotics (100 units/ml penicillin and 100 μg/ml streptomycin) in a humidified atmosphere of 5% CO_2 at 37 °C.

Myosin Heavy Chain Small-inhibitory RNAs (siRNA) Depletion—All sense and antisense siRNA oligos were synthesized by Dharmacon RNA Technologies and annealed. Target sequences for human myosin II isoforms are nonmuscle myosin heavy chain IIA (siIIA#1, TCTTGTGCTACTCTAGGA; siIIA#2, GATCAATCCATCTTGTGCA), nonmuscle myosin heavy chain IIB (siIIB#1, GACCACTGTGGACTCTAAA; siIIB#2, GTGGTATTACAGACATTCA), and firefly luciferase (GL2) for negative control. Transfection of siRNA (200 pmol) was performed using Oligofectamine reagent according to the manufacturer's protocol. Cells were ~30–40% confluent at the time of transfection. Assays were performed on the siRNA-depleted cells 96 h post-transfection, the time of maximum depletion. Cells were allowed to incubate with siRNA at least 24 h before changing media or replating for assays. All phenotypes examined were verified with both sets of siRNA, but all data shown were collected using siIIA#1 and siIIB#1, except where indicated.

Wound Healing Assay—Control and siIIA- and siIIB-transfected A549 cells were replated on plastic culture dishes 48 h post-transfection and cultured for an additional 48 h to produce a confluent monolayer. Wounds were made in the monolayer using a Cell Lifter (Costar #3008), producing a wound of ~250 μm. Loose cells were washed off, and fresh media was added to the cells immediately after wounding. Images were obtained of the wounds at various times after wounding using a Nikon CoolPix 5700 digital camera fitted to the eyepiece port of a Zeiss Axiovert 10 microscope using a MaxView Plus Adapter System from ScopeTronix (#STMVP). Images were imported into Adobe Photoshop CS, and wound widths were measured based on images of a 5-mm micrometer treated in the same manner. Distance migrated was calculated as the difference between the wound width at the time of the image and the initial wound width. Rate of wound closure was calculated as the slope of the linear regression of the plot of distance migrated *versus* time, combining the results from four separate experiments.

Video Microscopy—Videos of wound healing migration were made of wounds that were prepared in the same way as the wound healing assay, except the cells were replated onto fibronectin-coated (50 μg/ml) glass bottom microwell dishes (MatTek #P35G-0-10-C). Images of migrating cells were obtained every 5 min for 8 h (control and IIA-depleted cells) or 16 h (IIB-depleted cells) using a Zeiss axiovert 200 microscope equipped with a heated and humidified incubation chamber and a Hamamatsu ORCA-ER cooled charge-coupled device camera (Zeiss). Images were processed using Metamorph Image software (Universal Imaging). Time stamps were adjusted to reflect time after wounding. For videos of isolated cell migration the control, siIIA- and siIIB-transfected A549 cells were replated at low density onto fibronectin-coated (50 μg/ml) glass bottom microwell dishes 48 h post-transfection and cultured for an additional 48 h. Before imaging the medium was changed to Leibovitz's L-15 medium (Invitrogen #21083-027) supplemented with 10% heat-inactivated fetal bovine serum, 10 mM HEPES, and antibiotics. Images were acquired every 3 min for 2 h using a Nikon Eclipse TE2000-E microscope with a heated stage and a Nikon DXM 1200-F digital camera. Images were processed using Metamorph Image software (Universal Imaging).

Immunofluorescence Microscopy—Control and siIIA- and siIIB-transfected cells were replated on fibronectin-coated (50 μg/ml) 22 × 22-mm coverslips in 6-well plates 48 h post-transfection and cultured for an additional 48 h. Cells were fixed using 3% paraformaldehyde, 2% sucrose in phosphate-buffered saline (PBS) (pH 7) for 15–20 min and permeabilized with 0.2% Triton X-100 in PBS for 5 min. Nonspecific binding was blocked with 5% fetal bovine serum in phosphate-buffered saline plus 0.1% Triton X-100 followed by either a 1-h incubation at room temperature or an overnight incubation at 4 °C with the described anti-vinculin, anti-IIA, or anti-IIB antibodies diluted to 1:50–1:100 in blocking buffer followed by a 1-h incubation at room temperature with the appropriate fluorochrome-conjugated secondary antibodies. F-actin was labeled using rhodamine-conjugated phalloidin diluted to 33 nM in blocking buffer and incubated for 5–10 min. Coverslips were

mounted onto slides using Prolong Antifade (Molecular Probes #P7481) with 1 μg/ml 4′,6-diamidino-2-phenylindole to visualize DNA. Images were obtained on a Zeiss AxioImager.D1 coupled with a Zeiss AxioCam MRm monochrome cooled-CCD camera and analyzed with AxioVision software release 4.4.

Cell Spreading Assay—Control and siIIA- and siIIB-transfected A549 cells were released into a monocellular suspension using the non-trypsin Cellstripper solution (Cellgro #25-056-CI) 48 h post-transfection and replated (5×10^4) onto fibronectin-coated (50 μg/ml) 22 × 22-mm coverslips in 6-well plates and allowed to spread for an additional 48 h. These cells were then fixed, and F-actin was labeled with rhodamine-conjugated phalloidin as described above. For Rho kinase (ROCK) inhibition, wild type cells were incubated with Y-27632 (10 μM) for 2 h before fixation. Images of the phalloidin-stained cells were obtained on a Zeiss AxioImager.D1 coupled with a Zeiss Axio-Cam MRm monochrome cooled-CCD camera. The cell areas marked by phalloidin were traced and calculated using AxioVision software release 4.4. The histograms represent the combined data from three separate experiments, with 30 cells measured per experiment.

Cell Rounding Assay—Control and siIIA- and siIIB-transfected MDA-MB-231 cells (5×10^4) were replated on fibronectin-coated (50 μg/ml) 22 × 22-mm coverslips in 6-well plates 48 h post-transfection and cultured for an additional 48 h. The cells were starved of serum overnight (Dulbecco's modified Eagle's medium with 1% fatty acid-free bovine serum albumin, 10 mM HEPES, and antibiotics), which induced a flattened morphology. The cells were then treated with starvation media containing 1 unit/ml human α-thrombin (Enzyme Research Laboratories) for 30 min and immediately fixed in paraformaldehyde. To visualize the cells, F-actin was labeled with rhodamine-conjugated phalloidin, as described above. For ROCK inhibition, control siRNA-transfected cells were pretreated with 10 μM Y-27632 for 20 min before thrombin treatment. Images of four random high-power fields were obtained on a Zeiss AxioImager.D1 coupled with a Zeiss AxioCam MRm monochrome cooled-CCD camera, and the percent of rounded cells was determined. Data represent the mean ± S.E. from three separate experiments, with ~150 cells counted from each experiment.

Immunoprecipitation Assay—MDA-MB-231 cells (1.5×10^6) were plated in 10-cm culture dishes and grown to 80% confluency, then starved of serum overnight (Dulbecco's modified Eagle's medium with 1% fatty acid free bovine serum albumin, 10 mM HEPES, and antibiotics). Cells were then treated with thrombin (1 unit/ml) for 5 min with or without a 20-min pretreatment of 10 μM Y-27632. After thrombin treatment the cells were washed once with ice-cold phosphate-buffered saline followed by lysis in buffer C (50 mM Tris HCl (pH 7.5), 300 mM NaCl, 50 mM $Na_4P_2O_7$ (pH 6.75), 100 mM NaF, 1 mM EGTA, 2.5 mM ATP, 1% Triton X-100, 1 μM phenylmethylsulfonyl fluoride, 1 μM microcystin, 5 μg/ml leupeptin, and 10 μg/ml aprotinin). Cell lysates were briefly sonicated, then cleared by spinning for 10 min at 14,000 rpm at 4 °C in an Eppendorf centrifuge 5415 C. For immunoprecipitation, 800–1500 μg of total lysate was diluted to ~1.5–2 μg/μl with buffer C and incubated with either 5 μg of IIA or 10 μg of IIB antibody on a rocker overnight at 4 °C. After overnight incubation, 25 μl of a 1:3 slurry of pre-washed protein A-Sepharose CL-4B beads (GE Healthcare, formerly Amersham Biosciences #17-0780-01) were added and incubated for an additional 1.5 h on the rocker. The immuno-precipitates were washed 3 times with 300 μl of buffer C, then boiled in 3× SDS sample buffer for 5 min. The immunoprecipitates were separated by SDS-PAGE and subjected to immunoblot analysis. To make the loading across isoforms equivalent, ~25% of the immunoprecipitate loaded for IIB was loaded for IIA. For quantification of RLC phosphorylated on Ser-19 (P-RLC(Ser-19)) stimulation, the immunoblots were scanned and subjected to densitometry analysis using Odyssey v1.2 software. Loading was corrected by the amount of myosin II heavy chain in each lane. The corrected phosphorylation values from the thrombin ± Y-27632-treated samples were divided by the basal values from the starved, unstimulated samples to determine the -fold thrombin-induced phosphorylation. The data are represented as the mean of three separate experiments plus S.E.

In Vivo [^{32}P]Orthophosphate Labeling and Immunoprecipitation Assay—This immunoprecipitation assay was performed the same as above, except after overnight serum starvation the cells were incubated in phosphate-free media (Dulbecco's modified Eagle's medium without sodium phosphate (Invitrogen #11971-025) supplemented with 10 mM HEPES and antibiotics) for 2 h followed by labeling with 3 ml of phosphate-free media containing 1 mCi/ml [^{32}P]orthophosphate (GE Healthcare #PB-13) for 3 h. Cells were treated with thrombin with or without Y-27632 and lysed as described above except without sonication. After separation of the immunoprecipitates by SDS-PAGE, the gel was silver-stained and dried for PhosphorImager analysis. The amount of radioactivity incorporated into myosin IIA and IIB heavy chains, as well as the RLC was quantified using a PhosphorImager 445 SI scanner (GE Healthcare) along with IPLab Gel version 1.5 software (Signal Analytics Corp.). The radioactivity in each band was corrected by the amount of myosin II heavy chain immunoprecipitated, which was determined by densitometry analysis of the silver-stained gel using Odyssey Version 1.2 software. The corrected phosphorylation values from the thrombin ± Y-27632-treated samples were divided by the basal values from the starved, unstimulated samples to determine the -fold thrombin-induced phosphorylation. The data are represented as the mean of five separate experiments plus S.E.

Data Analysis—All data were analyzed using Statview 5.0.1 (SAS Institute Inc.). For the wound healing assay the regression for each treatment represents the combined data from four separate experiments. The differences between the regressions for each treatment were compared via analysis of covariance. For the cell spreading assay cell areas are represented both as histograms and as the means ± S.E. The histograms were analyzed first non-parametrically by the global Kruskal-Wallis test incorporating all variables followed by the Mann-Whitney *U* test for pairwise comparisons. All other results presented as the means ± S.E. were analyzed first by analysis of variance followed by Fisher's protected least significant difference to char-
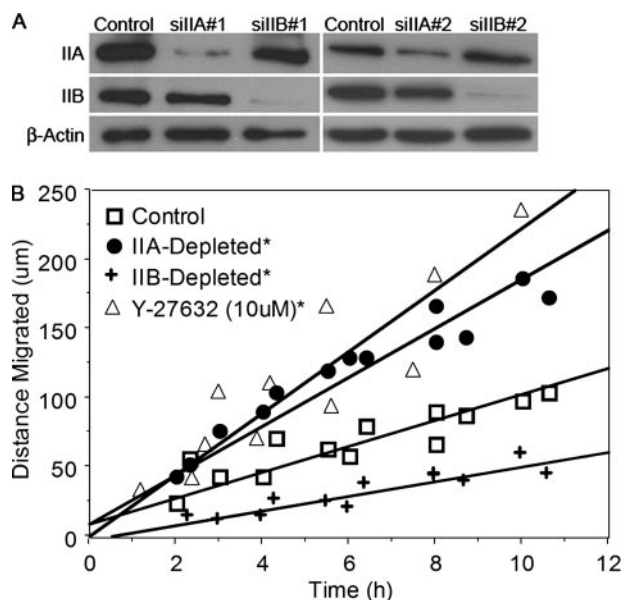
FIGURE 1. **IIA- and IIB-depleted A549 cells display opposite migration phenotypes.** *A*, Western blot analysis of A549 whole cell lysates demonstrating efficiency and specificity of isoform depletion. A549 cells were transfected with 200 pmol of siRNA directed against luciferase (*Control*), IIA (*siIIA*), or IIB (*siIIB*), and lysates were prepared 96 h post-transfection, the time of maximum depletion. Two siRNAs that were targeted to different regions of the transcript were designed for each myosin II isoform, and all phenotypes were verified using both sets of siRNA. Equal protein loading was verified by blotting for β-actin. *B*, Control and IIA- and IIB-depleted A549 cells were grown to confluency, and a wound was introduced into the monolayer 96 h post-siRNA transfection. Images of the wound were obtained at various time points after wounding, and the distance migrated was determined as described under "Experimental Procedures." To examine the effect of ROCK inhibition on wound healing, control cells were treated with Y-27632 (10 μM) for 20 min before wounding and throughout the assay. *Lines* represent the best-fit linear regressions of the combined results from three separate experiments. The rates of migration (slopes) for each cell type are as follows: control = 9.0 ± 0.5 μm/h, IIA-depleted = 18.0 ± 1.1 μm/h, IIB-depleted = 5.3 ± 0.6 μm/h; Y-27632-treated = 22 ± 3 μm/h (represented as the mean ± S.E.) *, All rates are statistically different from controls ($p < 0.0001$) by analysis of covariance, but the migration rates of IIA-depleted and Y-27632 treated cells are not statistically different.

acterize pairwise comparisons. Significance for all tests was assumed at $p < 0.05$.

RESULTS

siRNA Depletion of IIA or IIB Has Opposing Effects on Epithelial Cell Wound Healing Migration—When a wound is introduced into a monolayer of epithelial cells, the cells on both sides of the wound migrate coordinately as sheets in an effort to "close" the wound. To examine the distinct roles of IIA and IIB in epithelial sheet migration, we developed isoform-specific siRNAs to characterize the loss-of-function phenotypes associated with depletion of each isoform. Western blots of whole-cell extracts from cultured A549 cells (Fig. 1*A*) demonstrate that this cell line expresses both IIA and IIB and that we could successfully deplete one isoform without affecting the levels of the other isoform. To verify that the phenotypes observed with siRNA were specific, we designed two siRNAs for each isoform that targeted different regions of the mRNA transcripts. All phenotypes were reproduced with both siRNAs for each isoform.

We first characterized the effect depletion of IIA or IIB had on the ability of epithelial cells to perform wound healing

migration. Fig. 1*B* demonstrates that control cells (A549 cells transfected with siRNA directed against luciferase) reproducibly closed the wound at a rate of 9.0 ± 0.5 μm/h. siRNA depletion of IIA or IIB both resulted in changes in the rate of wound closure but, interestingly, the changes occurred in opposite directions. Specifically, IIA-depleted cells exhibited a 2-fold increase (18.0 ± 1.1 μm/h) in the rate of wound closure, whereas IIB-depleted cells covered the cell-free area at a rate ~60% that of control cells (5.3 ± 0.6 μm/h). The differences in the rate of wound closure for both the IIA- and IIB-depleted cells were statistically significant from that of the control cells ($p < 0.0001$). ROCK is a regulator of myosin II activity as it promotes RLC phosphorylation (21, 22). Thus, the small molecule inhibitor of ROCK, Y-27632 (23–25), has been used to examine the cellular functions of myosin II. Our data show that inhibition of ROCK with 10 μM Y-27632 resulted in an increase in the rate of A549 wound closure that was significantly different from control but not IIA-depleted cells (22 ± 3 μm/h). Small molecule inhibitors of ROCK in previous studies have had varied effects on cell migration, depending on cell type and migration model. Although ROCK inhibitors have been shown to decrease the transwell migration of PC3 prostatic carcinoma cells and human umbilical vein endothelial cells (26, 27), the increase in A549 cell wound closure rate observed with Y-27632 treatment here is consistent with reports demonstrating that inhibition of ROCK leads to increases in the rate of fibroblast wound migration (28).

IIA and IIB Distinctly Regulate Cellular Protrusions—In examining videos of control and IIA- and IIB-depleted cells migrating into a wound, we observed marked differences in membrane ruffling and lamellipodial protrusions between the cell types (Fig. 2 and supplemental Videos 1–3). Control cells entering the wound (Fig. 2 and supplemental Video 1) extended a generally broad, less phase-dense lamellipodial skirt that underwent repetitive periods of extension and retraction. IIA-depleted cells, however, exhibited a leading edge that was highly protrusive and one that retracted back toward the cell body less frequently than the control cells (Fig. 2 and supplemental Video 2). The lamellipodia of IIA-depleted cells also extended further into the wound, with extremely broad protrusions that often developed narrower, finger-like projections at the very front. In contrast, IIB-depleted cells exhibited diminished membrane ruffling and did not generate sustained protrusions (Fig. 2 and supplemental Video 3).

The distinct lamellipodia exhibited by the control and IIA- and IIB-depleted cells were examined further by fixation of cells migrating into a wound followed by visualization of the actin cytoskeleton via staining with rhodamine-conjugated phalloidin. The *top panel* of Fig. 3 demonstrates that the extended lamellipodia exhibited by control A549 cells contained bundles of F-actin, which most frequently formed parallel to the direction of protrusion (Fig. 3, *arrow* in *top panel*). The regions of the lamellipodia around these bundles stained brightly with phalloidin but appeared more diffuse, with little ultrastructure visible in the light microscope (Fig. 3, *arrowhead* in the *top panel*). This latter pattern of phalloidin staining is consistent with an organization of F-actin into a fine meshwork and is characteristic of lamellipodial protrusions (28). The leading edges of IIA-
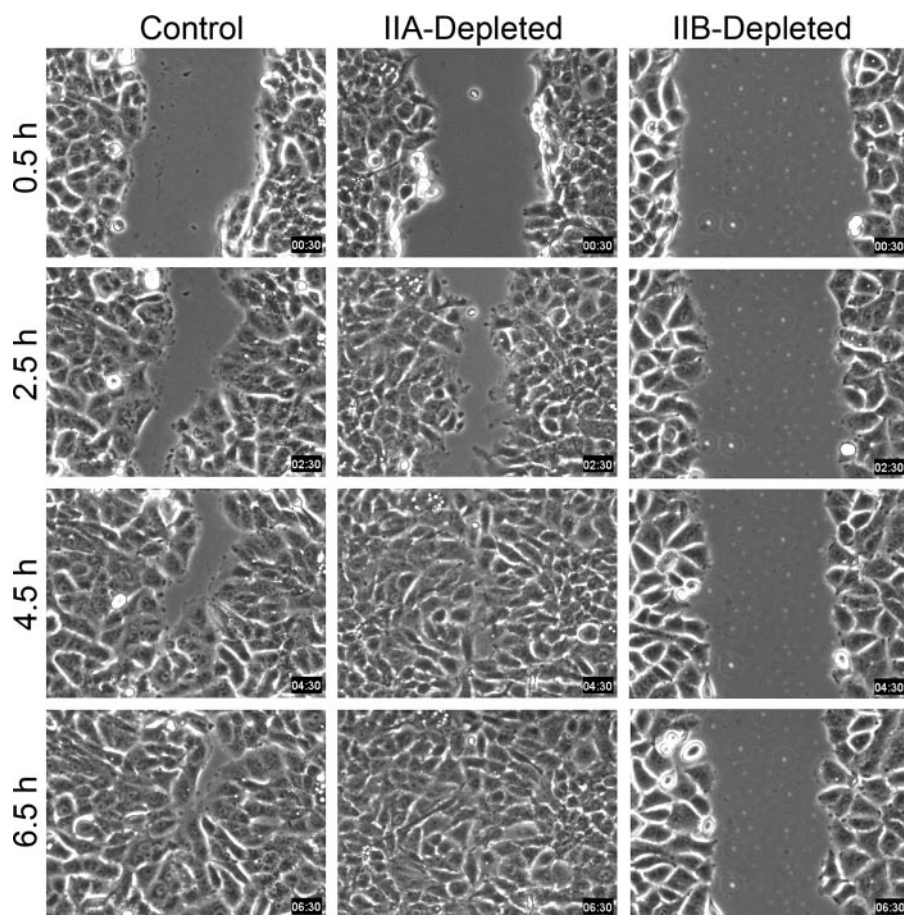
FIGURE 2. **Stills from supplemental videos of wound healing migration.** Control and IIA and IIB siRNA-transfected A549 cells were plated on fibronectin-coated (50 μg/ml), glass-bottomed 35-mm plates 48 h post-transfection and grown to a confluent monolayer. Wounds were introduced into the monolayer 96 h post-siRNA transfection. Phase/contrast images were obtained every 5 min for 8 h (*Control* and *IIA-depleted*) or 16 h (*IIB-depleted*) post-wounding. Images comprise a series of video stills at 0.5, 2.5, 4.5, and 6.5 h post-wounding demonstrating differences in the rate of wound closure. See also supplemental Videos 1–3.

migration and protrusion phenotypes observed in the wound healing assay.

Previous studies have demonstrated that inhibition of Rho-ROCK signaling and myosin II activity result in increased cellular protrusions all around the cell, leading to the hypothesis that Rho-ROCK signaling, in conjunction with myosin II contractility, is required to restrict protrusions to the leading edge (24, 30). Under this hypothesis, cells in which myosin II activity is absent would protrude dynamically on all sides. However, in a wound, protrusions can protrude only in one direction, into the wound. We, therefore, made time-lapse videos of sparsely plated, isolated cells to examine their protrusions. As predicted, IIA-depleted cells showed dynamic protrusions on all sides of the cell, with little net movement of the cell body (Fig. 5 and supplemental Video 5). This was in contrast to control cells, which demonstrated more persistent protrusions and in which translocations of the entire cell body were common (Fig. 5 and supplemental Video 4). As expected, the IIB-depleted cells exhibited little movement or protrusional activity (Fig. 5 and supplemental Video 6).

Taken together the above data suggest that IIA and IIB both perform important but distinct roles in regulating cell protrusions during cell migration.

siRNA Depletion of IIA or IIB Results in Unique Changes in Focal Adhesions—Myosin II-based contractility, via contraction of F-actin into stress fiber bundles, is required for the assembly of focal adhesions (12). Because changes in substrate adhesion are known to modulate cellular protrusions (31), one hypothesis to explain the distinct protrusion phenotypes observed in IIA- and IIB-depleted cells is through differential regulation of focal adhesions by IIA and IIB. Accordingly, we examined the focal adhesions and stress fibers formed in control and IIA- and IIB-depleted and Y-27632-treated cells by dual staining for the focal adhesion protein vinculin and F-actin. Fig. 6 shows that control A549 cells cultured on fibronectin exhibit punctate vinculin staining, indicative of focal adhesions, throughout the cell cortex and most strongly in the cell periphery. These focal adhesions anchored actin stress fibers, as evidenced by the *yellow* punta in the merge of the vinculin and phalloidin staining (Fig. 6, see *Merge*). IIA-depleted and 10 μM Y-27632-treated cells both exhibited a more diffuse, cytoplasmic pattern of vinculin staining that was most intense around the nucleus and diminished toward the periphery. And unlike

depleted cells displayed few to no bundles of F-actin, and the lamellipodia were very broad and thin compared with those of the control cells (Fig. 3, *middle panel*). At the other extreme, the lamellipodia extended by the IIB-depleted cells were small (Fig. 3, *arrow* in *bottom panel*). Furthermore, these cells formed prominent bundles of F-actin that ran along the leading edge, parallel to the wound (Fig. 3, *arrowhead* in *bottom panel*), rather than orthogonal to the wound as in the control cells.

The cytoskeletal dynamics that occur during cell spreading are commonly considered to be similar to the events occurring at the leading edge of migrating cells (29); thus, we also examined the effects of IIA or IIB depletion as well as Y-27632 treatment on the ability of A549 cells to spread on fibronectin. An examination of the distribution of control cell areas after spreading revealed a bell-shaped curve that skewed slightly to the right and averaged 1820 $\pm$ 65 um^2 (Fig. 4). Consistent with their decreased migration and more retractile morphology, IIB-depleted cells were significantly less well spread than the controls with a mean cell area of 1100 $\pm$ 49 um^2. In contrast, the spread areas of cells depleted of IIA or treated with Y-27632 were both significantly skewed to the right, demonstrating mean cell areas of 2380 $\pm$ 78 and 2620 $\pm$ 91 um^2, respectively. These cell-spreading phenotypes correlate strongly with the
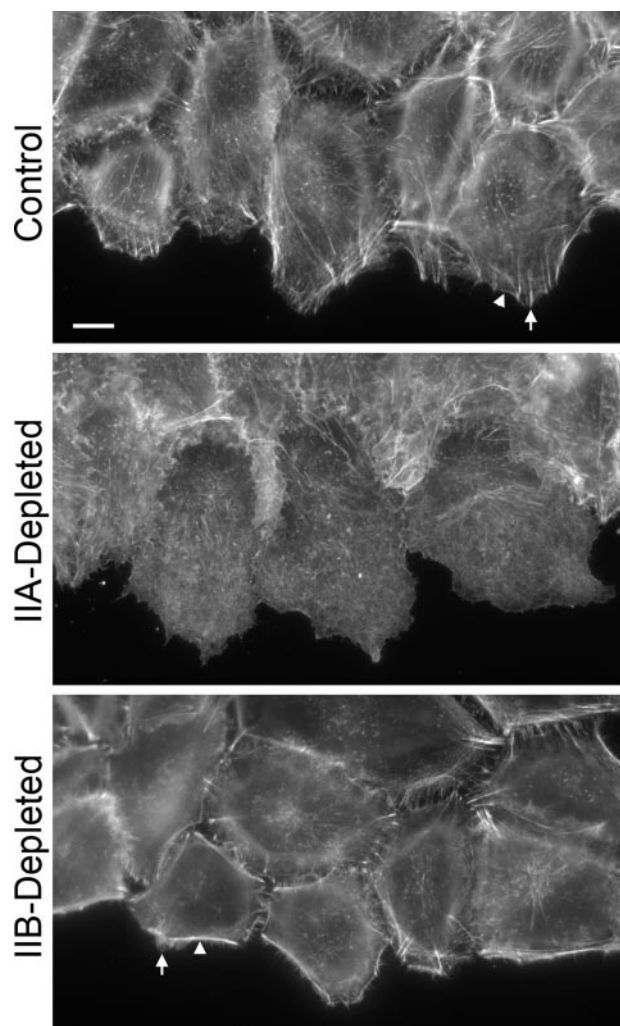
FIGURE 3. **Leading edge morphologies of IIA- and IIB-depleted cells.** Control and IIA- and IIB-depleted A549 cells were grown to a confluent monolayer on fibronectin-coated (50 μg/ml) glass coverslips. A wound was introduced into the monolayer 96 h post-siRNA transfection, and the cells were allowed to migrate into the wound for 90 min, then fixed with paraformaldehyde and stained with rhodamine-conjugated phalloidin to visualize F-actin. *Arrows* indicate bundles of F-actin, and the *arrowheads* indicate areas of protrusion. *Scale* = 10 μm.

FIGURE 4. **IIA-depleted cells exhibit increased cell spreading, whereas IIB-depleted cells are retractile.** Control and IIA- and IIB-depleted A549 cells were released into suspension using the non-trypsin-based Cellstripper solution (see "Experimental Procedures") 48 h post-siRNA transfection, then replated in full serum on fibronectin-coated (50 μg/ml) glass coverslips. These cells were then allowed to attach and spread for an additional 48 h. After spreading, the cells were paraformaldehyde-fixed, and F-actin was labeled using rhodamine-conjugated phalloidin. For ROCK inhibition wild type cells were incubated with Y-27632 (10 μM) for 2 h before fixation. Cell areas were determined as described under "Experimental Procedures." Histograms demonstrating the distribution patterns of cell areas of asynchronous populations are shown and represent the combined data from three experiments with ~30 cells/experiment measured. *, non-parametric analysis of the data demonstrated that distribution of IIA- and IIB-depleted cells as well as Y-27632-treated cells were significantly different from that of the control cells ($p < 0.0001$). #, the average cell areas are also significantly different from control cells ($p < 0.0001$). Note that a significant difference did not exist between IIA-depleted and Y-27632 treated cells.

control cells, few to no focal adhesions were observed, although the smaller, Rac-regulated focal complexes (30, 32) may still be present, especially in the peripheral regions. These cells were also nearly devoid of stress fibers but did occasionally display some bundled F-actin (Fig. 6). In addition, the IIA-depleted and Y-27632-treated cells exhibited a more protrusive morphology, which along with the changes in focal adhesions and stress fibers, is consistent with previous descriptions of decreased Rho-ROCK-mediated contractility (24, 28). In the IIB-depleted cells focal adhesions were observed; however, they were restricted to the cell perimeter. IIB-depleted cells were retractile and polygonal in morphology, with prominent bundles of F-actin running the perimeter of the cells, terminating in the peripheral focal adhesions (Fig. 6, see *Merge*). These data strongly suggest that IIA and IIB differentially contribute to focal adhesion formation and/or maintenance. Furthermore, the observation that IIA- but not IIB-depleted cells exhibit a lack of focal adhesions and stress fibers similar to that of
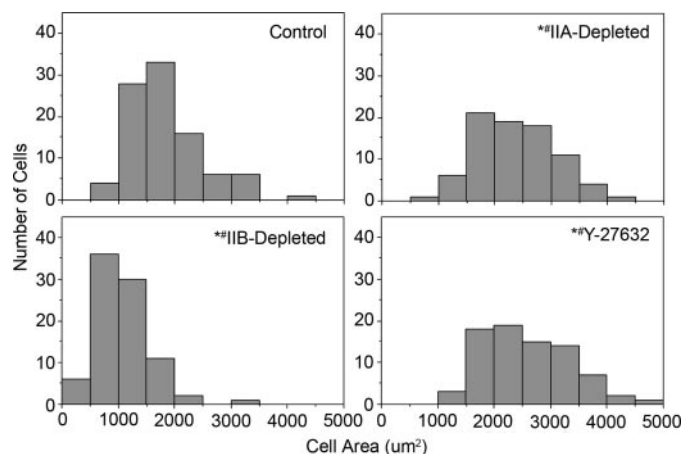
Y-27632-treated cells suggests that IIA is specifically required for Rho-induced contractility.

IIA and IIB Exhibit Distinct Subcellular Localization Patterns—Many previous studies have examined the subcellular localization patterns of IIA and IIB, with a broad range of cell type-specific distributions having been described (33–36). What is consistent is that IIA and IIB display differences in their distributions, especially in motile cells. In A549 cells cultured on fibronectin, both IIA and IIB appeared as puncta distributed throughout the cytoplasm, with these puncta occasionally organizing into linear arrays that coincide with stress fibers (Fig. 7, *A* and *B*, see *Merge*). IIA appeared to associate more strongly with stress fibers, however, as indicated by the yellow coloring of the merge between IIA and phalloidin staining (Fig. 7*A*). Close examination of IIA staining revealed that this isoform distributed broadly throughout the cytoplasm, extending nearly to the very leading edge (Fig. 7*A*). Furthermore, IIA commonly co-localized with focal adhesions, with the linear arrays of IIA staining often terminating in vinculin-containing structures (Fig. 7*B*, *arrows*). IIB staining, however, was observed most strongly in the rear and along the sides of cells, where they were not protruding, and overlapped with F-actin in these regions. In areas of protrusions, both in isolated cells (Fig. 7*B*) or polarized cells along the edge of a wound (Fig. 7*A*), IIB staining was less intense. Thus, in polarized cells IIA appeared enriched in the lamellipodia relative to IIB. Unlike IIA, IIB staining lacked intensity in areas where focal adhesions were in abundance and did not generally merge with vinculin staining, which is especially visible in the leading edge of the cell (Fig. 7*B*, *arrows*).
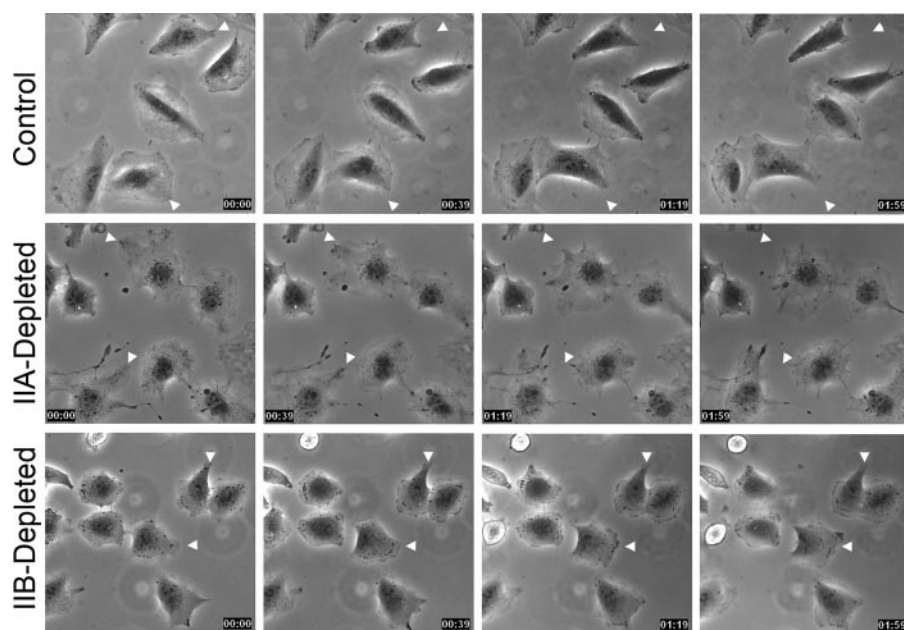
FIGURE 5. **Protrusional activities of isolated control, IIA-and IIB-depleted cells are distinct.** Control and IIA- and IIB-depleted cells were replated on fibronectin-coated (50 μg/ml) glass-bottomed dishes 48 h post-siRNA transfection and cultured for an additional 48 h. The protrusion activities of each cell type were then examined by acquiring time-lapse phase/contrast images of the same view field every 3 min for 2 h. Shown here are images obtained at 0, 19, 79, and 119 min (from *left* to *right* in each *row*). *Arrowheads* serve as reference points to follow the morphological changes for each cell type. Note that control cells exhibit sustained protrusions and cell body translocations. IIA-depleted cells, however, are much more dynamic, first protruding in one direction followed by retraction and protrusion in a new direction, with little net movement of the cell body. IIB-depleted cells exhibit only minor changes in morphology over the same 2-h time period. See supplemental Videos 4–6.

Interestingly, under the light microscope, IIA staining occasionally exhibited an area of low intensity that was coincident with the nucleus, which was not observed as often with IIB staining (Fig. 7*B*). A careful analysis of IIA and IIB staining patterns with a confocal microscope would provide further interesting information about the differential localizations of these isoforms. However, in general, the localization patterns of both myosin II isoforms in A549 cells observed here are consistent with those previously described in endothelial cells (36, 37).

IIA but Not IIB Is Required for ROCK-mediated, Thrombin-induced Cell Rounding—In all the above phenotypes, IIA-depleted cells were comparable with cells in which ROCK activity was inhibited (Figs. 1, 5, and 6). This correlation suggests that IIA is specifically required for contractile events downstream of the Rho-ROCK signaling pathway in a way that is consistent with the classically described functions of myosin II. To characterize this more carefully, we examined the specific contributions of IIA and IIB to another process in which myosin II contractility is required downstream of Rho-ROCK signaling, namely thrombin-induced cell rounding (5, 38, 39). Serum-starved MDA-MB-231 cells display a flattened morphology; however, after thrombin treatment the cells round up and undertake a spherical shape (Fig. 8*B*). Thirty minutes after stimulation of starved MDA-MB-231 cells with 1 unit/ml thrombin, 57 $\pm$ 4% of the control cells have undergone cell rounding (Fig. 8*C*). MDA-MB-231 cells, either depleted of IIA or treated with 10 μM Y-27632, exhibited an equivalent, statistically significant block ($p < 0.0001$) in cell rounding, with only

15 $\pm$ 1 and 13 $\pm$ 2% of these cells responding to thrombin, respectively (Fig. 8*C*). IIB is not required for cell rounding, and in fact a higher percentage of IIB-depleted cells were round (72 $\pm$ 3%, $p < 0.006$) after thrombin treatment when compared with control cells. This observation, when considered along with the data from Figs. 3–5, demonstrating that IIB-depleted cells are less-well spread and exhibit fewer protrusions than control cells, suggests that cells depleted of IIB display a higher propensity to undergo retraction than extension. Furthermore, these data support the idea that IIA is specifically required for contractile events downstream of Rho-ROCK signaling.

ROCK Differentially Regulates Phosphorylation of the RLC Associated with IIA and IIB—The above data demonstrate that IIA and IIB perform distinct functions in the cell. However, how these isoforms are regulated differently is unclear. Myosin II activity is regulated in large part through phosphorylation of the RLC, with Ser-19 of the RLC considered to be the major site of phosphorylation (2, 40, 41). Phosphorylation at Ser-19 both increases the actin-activated ATPase activity of myosin II and promotes myosin II filament assembly. Multiple kinases have been shown to be able to phosphorylate Ser-19, including myosin light chain kinase, ROCK, p21-activated kinase, and zipper-interacting protein kinase (21, 42–44). Furthermore, ROCK has been shown to regulate the phosphorylation of the RLC directly (21) as well as indirectly by phosphorylation and inhibition of the targeting subunit of the RLC phosphatase, MYPT-1 (22, 45). However, whether ROCK or any kinase differentiates between the RLC specifically associated with IIA and IIB (hereafter, IIA-RLC and IIB-RLC, respectively) has not been carefully examined. Thus, one mechanism of isoform-specific regulation that could account for the observed correlation between IIA depletion and ROCK inhibition is a differential regulation of IIA- and IIB-RLC phosphorylation by ROCK, with the kinase preferentially regulating IIA-RLC phosphorylation.

To examine whether ROCK differentiates between IIA- and IIB-RLC, we immunoprecipitated IIA and IIB with isoform-specific antibodies and characterized the thrombin-induced changes in phosphorylation of the RLC that co-immunoprecipitated specifically with each heavy chain isoform. This immunoprecipitation assay was performed on lysates prepared from MDA-MB-231 cells that were starved and treated with thrombin in the presence or absence of Y-27632, similar to the cell rounding assay. Fig. 9*A* shows the immunoblot analysis of IIA and IIB immunoprecipitates from MDA-MB-231 cells treated with thrombin alone (*T*), thrombin plus Y-27632
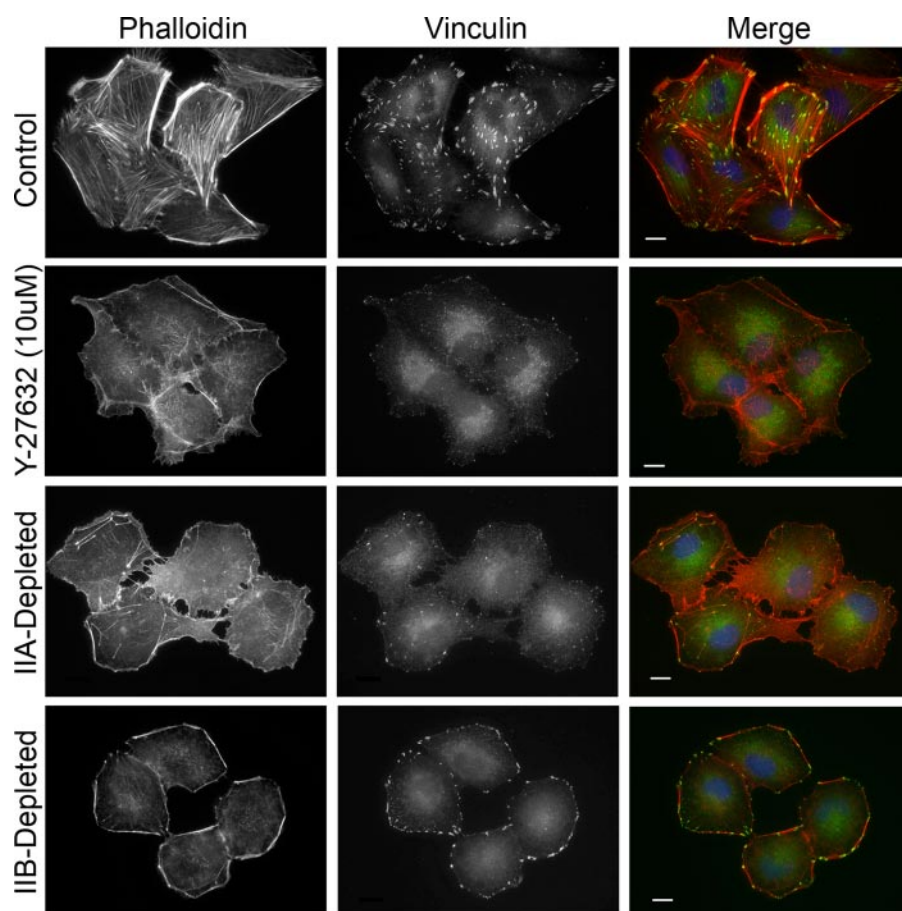
FIGURE 6. **IIA- and IIB-depleted cells exhibit distinct focal adhesion phenotypes.** Control and IIA- and IIB-depleted A549 cells were plated on fibronectin-coated (50 μg/ml) glass coverslips 48 h post-siRNA transfection and cultured for an additional 48 h. The cells were then paraformaldehyde fixed and immunostained with anti-vinculin monoclonal antibody (*green*) to mark focal adhesions and rhodamine-conjugated phalloidin (*red*) to label F-actin. For ROCK inhibition, control siRNA-transfected cells were treated with Y-27632 (10 μM) for 2 h before fixing. In the merge 4′,6-diamidino-2-phenylindole (*blue*) labels DNA. *Scale* = 10 μm.

($T+Y$), or left untreated (*U*). The immunoblots of IIA and IIB heavy chains with the isoform specific antibodies demonstrate that equivalent amounts of IIA or IIB were immunoprecipitated across treatments; however, the amount of IIB immunoprecipitated was consistently low compared with IIA. Furthermore, immunoprecipitation was specific for each isoform, as no IIB was detected in the IIA immunoprecipitates, and vice versa (data not shown).

We next probed the IIA and IIB immunoprecipitates with a phospho-specific antibody that specifically recognizes P-RLC(Ser-19) to examine whether ROCK differentially regulates the phosphorylation of IIA- and IIB-RLC at that site in response to thrombin. Fig. 9*A* shows that thrombin induced an increase in phosphorylation at Ser-19 on IIA-RLC and that this phosphorylation was completely inhibited by pretreatment with 10 μM Y-27632. A similar result was observed when using an antibody that recognizes RLC doubly phosphorylated on residues threonine 18 and serine 19 (data not shown). Treatment of these cells with thrombin ± Y-27632 induced a similar trend in IIB-RLC phosphorylation at Ser-19 as on IIA-RLC. However, the thrombin-induced stimulation of IIB-RLC phosphorylation was consistently weaker than that observed on IIA-RLC, and when quantified by densitometry, the mean -fold

stimulation of IIB-RLC phosphorylation was less than two-thirds that of IIA-RLC (Fig. 9*B*).

As a more sensitive measure of changes in phosphorylation, we repeated the immunoprecipitation assay after first labeling the cells *in vivo* with radioactive [^{32}P]orthophosphate. Besides being a more sensitive method, labeling cells with radioactive phosphate enabled us to examine whether ROCK differentially regulated the phosphorylation of IIA and IIB on any site, including any on the heavy chain. This assay was performed in the same way as the above immunoprecipitation assay, except that the cells were first incubated with 1 mCi/ml [^{32}P]orthophosphate before treatment with thrombin or Y-27632. The immunoprecipitates were separated by SDS-PAGE, and the amount of radioactive phosphate that was incorporated into IIA and IIB heavy chains as well as IIA- and IIB-RLCs was determined by PhosphorImager analysis. A silver stain of the gel (Fig. 9*C, top panel*) demonstrates that equivalent amounts of IIA and IIB were immunoprecipitated across treatments. Again, less IIB was consistently immunoprecipitated compared with IIA, and to make the loading across isoforms equivalent, ~25% of the immunoprecipitate loaded for IIB was loaded for IIA. The amounts of IIA and IIB that were immunoprecipitated and loaded on the gel were quantified by densitometry and used for normalization. Quantification of the radioactivity incorporated into IIA and IIB heavy chains by PhosphorImager analysis revealed that IIB was labeled with higher amounts of radioactivity than IIA heavy chain, even in the unstimulated sample (data not shown). This is consistent with reports from the literature, as several more sites of phosphorylation have been reported in the C-terminal tail region of the IIB heavy chain compared with the homologous region of the IIA heavy chain (2, 46). Despite the presence of detectable levels of phosphorylation on both IIA and IIB in the basal state, treatment with thrombin and/or Y-27632 did not have a significant effect on the amount of radioactive phosphate that was incorporated into either heavy chain (data not shown).

A representative PhosphorImager scan of IIA- and IIB-RLC phosphorylated with radioactive phosphate is shown in the *bottom panel* of Fig. 9*C*. This assay was repeated fives times, and the -fold increase in RLC phosphorylation induced by thrombin over the basal level of phosphorylation in the unstimulated sample was determined for both IIA- and IIB-RLC. The *bar graph* in Fig. 9*D*, similarly to Fig. 9*B*, demonstrates that whereas
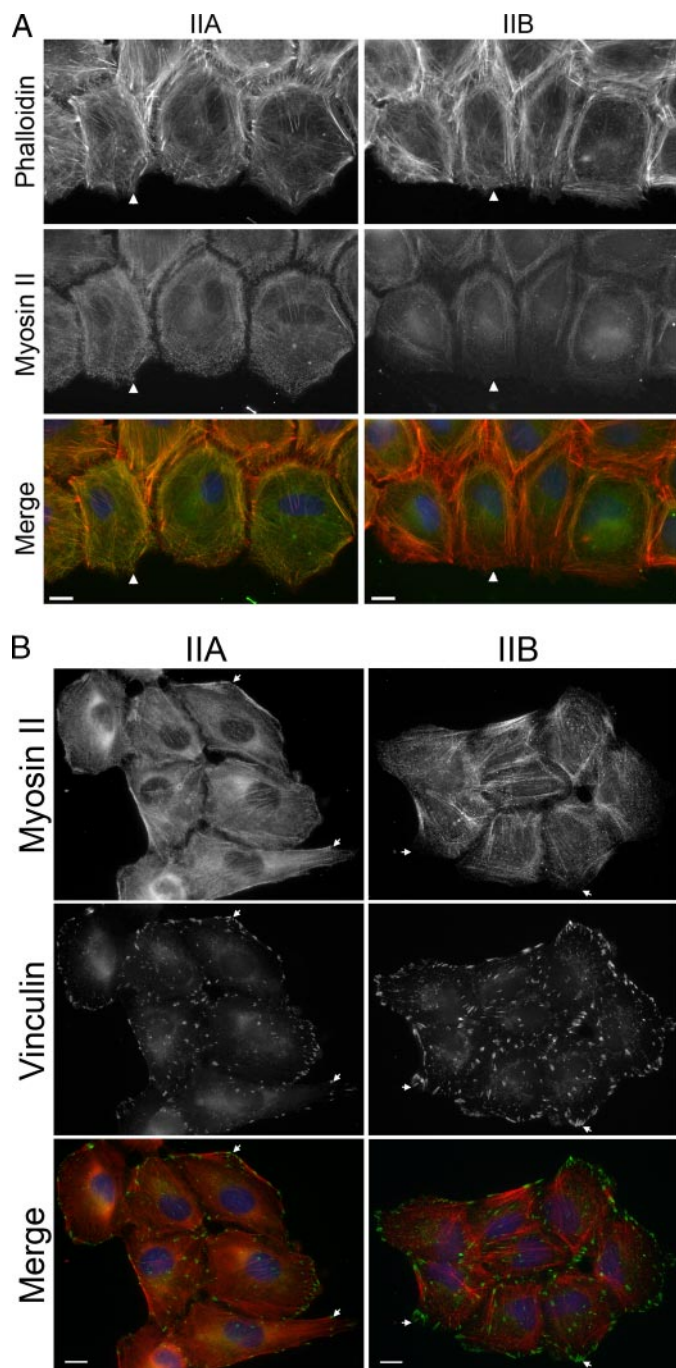
FIGURE 7. **IIA and IIB exhibit distinct subcellular localizations.** *A*, IIA and IIB localizations in polarized cells on the edge of a wound. A549 cells were plated on fibronectin-coated (50 μg/ml) glass coverslips and cultured for 48 h to confluency. The monolayer was wounded, and the cells were allowed to migrate for 60 min. The cells were then paraformaldehyde-fixed and immunostained with polyclonal antibodies that are specific to IIA (*green*, *left column*) or IIB (*green*, *right column*) to mark the myosins and rhodamine-conjugated phalloidin to visualize F-actin (*red*). In the merge 4′,6-diamidino-2-phenylindole (*blue*) labels DNA. *Scale* = 10 μm. *Arrowheads* indicate areas of leading edge protrusion. Note that IIA staining is prominent in the lamellipodia, whereas IIB staining is most intense in the rear of the cells. *B*, IIA and IIB localizations in isolated cells. A549 cells were plated sparsely on fibronectin-coated (50 μg/ml) glass coverslips for 48 h, then paraformaldehyde-fixed and immunostained with an anti-vinculin monoclonal antibody to mark focal adhesions (*green*) and polyclonal antibodies that are specific to IIA (*red*, *left column*) or IIB (*red*, *right column*) to mark the myosins. In the merge 4′,6-diamidino-2-phenylindole (*blue*) labels DNA. *Scale* = 10 μm. *Arrows* indicate areas of focal adhesion, where IIA staining is present, but IIB staining is weak.
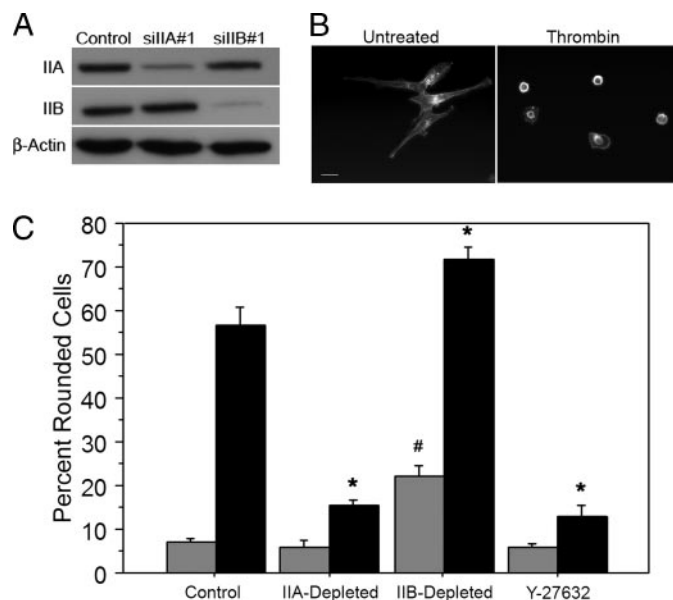

FIGURE 8. **IIA-depleted and Y-27632-treated cells are deficient in thrombin-induced cell rounding.** *A*, Western blots of MDA-MB-231 whole cell lysates prepared 96 h post-siRNA transfection, demonstrating that although less transfectable than A549 cells, siRNA depletion of IIA and IIB is achievable in this cell line. *B*, representative phase/contrast images of control MDA-MB-231 cells with and without 1 unit/ml thrombin treatment. *Scale* = 20 μm. *C*, control and IIA- and IIB-depleted MDA-MB-231 cells were plated on fibronectin-coated (50 μg/ml) glass coverslips. After overnight serum starvation the cells display a flattened morphology. The cells were then treated with 1 unit/ml thrombin (*black bars*) or left untreated (*gray bars*) for 30 min and immediately paraformaldehyde-fixed. To visualize the cells, F-actin is labeled with rhodamine-conjugated phalloidin. Images of four random high-power fields were obtained, and the percent of rounded cells was determined. Data represent the mean ± S.E. from three separate experiments, with ~150 cells counted from each experiment. *, percent rounded cells after thrombin treatment is significantly different from control cells ($p < 0.006$). #, percent rounded cells without thrombin is significantly different from control cells ($p < 0.002$).

thrombin stimulated phosphorylation of the RLC associated with both myosin II isoforms, the stimulation on IIB-RLC was ~50% that of IIA-RLC. Furthermore, pretreatment with Y-27632 completely inhibited the thrombin-induced phosphorylation. Taken together these data suggest that thrombin preferentially induces phosphorylation of IIA-RLC, which is mediated through the Rho-ROCK signaling cascade. This result is consistent with the observation that IIA is selectively required for thrombin-induced cell rounding and provides support for the hypothesis that IIA and IIB can be regulated by distinct signaling pathways.

DISCUSSION

The importance of myosin II for cellular contractile processes has been well documented. However, until recently little was known about the unique cellular functions of the different myosin II isoforms, IIA and IIB. Data presented here demonstrate that, indeed, IIA and IIB are both required for normal migration but in distinct ways. Surprisingly, siRNA depletion of each isoform resulted in opposite migratory phenotypes, with IIA- and IIB-depleted cells exhibiting rates of wound healing migration at ~200 and 60% that of control cells, respectively (Fig. 1*B*). Furthermore, cells depleted of IIA exhibited decreases in stress fibers and focal adhesions, with concomitant increases
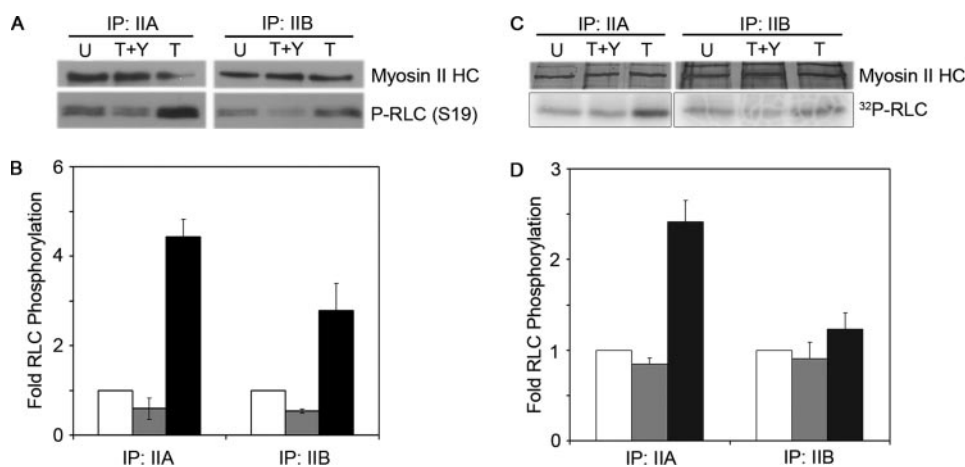
FIGURE 9. **ROCK preferentially regulates phosphorylation of RLC associated with IIA.** MDA-MB-231 cells were plated in 10-cm culture dishes and grown to 80% confluency, then starved of serum overnight. Cells were then treated with thrombin (1 unit/ml) for 5 min with or without a 20-min pretreatment of Y-27632 (10 μM). IIA and IIB were immunoprecipitated using isoform-specific polyclonal antibodies followed with separation by SDS-PAGE. *A*, Western blot of IIA and IIB immunoprecipitates (*IP*) using the isoform-specific antibodies (IIA and IIB) and a phospho-specific polyclonal antibody that recognizes the RLC phosphorylated at Ser-19 (*P-RLC (S19)*). Note that the film exposure time for the P-RLC(Ser-19) blot of the IIB immunoprecipitate is 10 times longer than that for IIA. *B*, *bar graph* representing a quantification of the -fold RLC phosphorylation in thrombin (*T*, *black*) or thrombin plus Y-27632 (*T+Y*, *gray*) immunoprecipitates over untreated (*U*, *white*) samples without thrombin stimulation. The amount of RLC phosphorylation at Ser-19 was quantified by densitometry for three immunoblots and corrected by the amount of myosin II heavy chain immunoprecipitated. All three immunoblots showed similar trends, and these data represent the mean of the three experiments plus S.E. *C* and *D*, [^{32}P]orthophosphate labeling followed by IIA and IIB immunoprecipitation. Assay performed essentially the same as in *A*, except the cells were first incubated in phosphate-free media for 2 h followed by labeling with phosphate-free media containing [^{32}P]orthophosphate (1 mCi/ml) for 3 h before thrombin treatment. *C*, representative gel of silver-stained myosin II heavy chain (*top*) and PhosphorImager scan of the radioactivity incorporated into the RLC (*bottom*). Note that to make the loading across isoforms equivalent, ~25% of the immunoprecipitate loaded for IIB was loaded for IIA. *D*, *bar graph* representing the amount of radioactivity incorporated into the RLC as quantified by PhosphorImager analysis and corrected by the amount of myosin II heavy chain immunoprecipitated. Each *bar* represents the -fold RLC phosphorylation in thrombin (*T*, *black*) or thrombin plus Y-27632 (*T+Y*, *gray*) immunoprecipitates over untreated (*U*, *white*) samples without thrombin stimulation. Data represent the mean plus S.E. of five similar experiments.

in cell protrusions, whereas IIB-depleted cells were at the opposite end of the spectrum. With few protrusions and less spreading on fibronectin, cells depleted of IIB exhibited a higher tendency toward retraction than extension. The phenotypes observed with IIA depletion are consistent with the generally accepted functions of myosin II downstream of Rho-ROCK signaling (12, 24, 28, 47). Namely, Rho-ROCK-mediated myosin II contractility promotes stress fiber and focal adhesion formation and is inhibitory to protrusion. Thus, one interpretation of our data is that loss of IIA-based contractility relieves a restriction on protrusions, whereas IIB has a limited role in protrusion regulation. However, the observation reported here that IIB-depleted cells are less well spread compared with control cells suggests that IIB activity indeed facilitates cellular protrusions.

Because it is generally accepted that the force required to produce membrane protrusions is generated by actin polymerization (48, 49), our data raise the question as to how IIA and IIB distinctly regulate cell protrusions. In light of the observations that the protrusion as well as cell rounding phenotypes of IIA- and IIB-depleted cells are opposite in nature (see Figs. 4 and 8), one simple hypothesis is that IIA and IIB contractility counteract each other. Thus, depletion of one isoform would result in a shift in the balance of IIA- *versus* IIB-based contractility, resulting in the opposing phenotypes. Alternatively, it is known that changes in substrate adhesion can modulate cell protrusions (31) and that myosin II-mediated contractility is required

for focal adhesion assembly (12). Therefore, the distinct ways in which IIA and IIB regulate focal adhesions (Fig. 6) may contribute to the different protrusive phenotypes, although the mechanism for this remains unclear. Perhaps IIA and IIB do the same thing, simply in different places. Support for this hypothesis can be drawn from the distinct distributions of IIA and IIB (Figs. 7, *A* and *B*). For instance, because IIB is of relatively low abundance compared with IIA in the cell periphery, IIB-depletion would be expected to have little effect on the assembly of peripheral focal adhesions. Alternatively, because the adhesive complexes necessary for cell motility are heterogeneous structures that exhibit a dynamic life cycle consisting of periods of assembly, maturation/maintenance, and disassembly (50, 51), it is possible that IIB is selectively required for some other aspect of focal adhesion regulation, such as their centripetal translocations (14, 52). In the latter scenario, the absence of IIB would again result in an abundance of focal adhesions at the cell periphery. A thorough characterization of focal adhesion dynamics in live cells will be instrumental to our complete understanding of the different roles IIA and IIB play in adhesion and protrusion regulation.

Despite our observations that IIA and IIB perform distinct cellular functions, it remains unclear why cells express multiple myosin IIs, since each isoform appears to perform the same basic molecular function. In considering this question, observations made from some cell types that are naturally enriched for, or solely express a single isoform may offer important insight. For instance, only IIA is detected in platelets (35, 53), and the shape change necessary for platelet activation requires myosin II-based contractility (4, 54). This large scale contractile process is similar to thrombin-induced rounding of MDA-MB-231, which specifically requires IIA and not IIB. Thus, IIA may be better suited for large scale contractile processes than IIB. Support for this idea can be drawn from the observations that IIA localizes broadly throughout the cytoplasm and that this isoform moves actin at nearly three times the rate of IIB (33). Conversely, IIB is enriched in neurons (34, 53), where a more restrictive localization pattern and less powerful motor may provide more delicate regulation of contraction, supporting the complex process of neurite extension. The two cell types used in this study express both myosin II isoforms, with IIA being expressed at a higher level compared with IIB, similar to what has been reported for endothelial cells (36). This suggests that migrating cells require a balance of both myosin II isoforms to

provide the proper contractile forces necessary at different places in the cell at the proper time during the migration process.

Last, our data as well as previous work by others provide strong evidence supporting the idea that IIA and IIB perform unique cellular functions. However, exactly how the cell regulates IIA and IIB functions separately is not yet clear. Our data support a role for ROCK in the preferential regulation of IIA-RLC phosphorylation and are consistent with the strong correlation observed between ROCK inhibition and IIA-depletion. This raises the question as to how the cell specifically regulates IIB activity. The most obvious hypothesis is that one or more of the multiple other RLC kinases regulate IIB activity. Indeed, Totsukawa *et al.* (23) demonstrated that myosin light chain kinase and ROCK can regulate the phosphorylation of discrete pools of RLC in different sub-cellular locales. Moreover, although thrombin did not induce a significant change in heavy chain phosphorylation on either isoform, epidermal growth factor treatment has been shown to be important for regulating IIB heavy chain phosphorylation and IIB activity (55, 56), representing another mode of potential isoform specific regulation. Regulation of IIA and IIB by distinct pathways is an attractive idea that could explain how myosin II performs its many functions at different places in the cell at different times. Much more work is required for a complete understanding of the specific cellular roles of IIA and IIB, and how the activities of these isoforms are distinctly regulated by the cell.

REFERENCES

1. Sellers, J. R. (2000) *Biochim. Biophys. Acta* **1496,** 3–22
2. Bresnick, A. R. (1999) *Curr. Opin. Cell Biol.* **11,** 26–33
3. Satterwhite, L. L., and Pollard, T. D. (1992) *Curr. Opin. Cell Biol.* **4,** 43–52
4. Daniel, J. L., Molish, I. R., Rigmaiden, M., and Stewart, G. (1984) *J. Biol. Chem.* **259,** 9826–9831
5. Majumdar, M., Seasholtz, T. M., Goldstein, D., de Lanerolle, P., and Brown, J. H. (1998) *J. Biol. Chem.* **273,** 10099–10106
6. Warrick, H. M., and Spudich, J. A. (1987) *Annu. Rev. Cell Biol.* **3,** 379–421
7. Wessels, D., Soll, D. R., Knecht, D., Loomis, W. F., De Lozanne, A., and Spudich, J. (1988) *Dev. Biol.* **128,** 164–177
8. Mitchison, T. J., and Cramer, L. P. (1996) *Cell* **84,** 371–379
9. Ridley, A. J., Schwartz, M. A., Burridge, K., Firtel, R. A., Ginsberg, M. H., Borisy, G., Parsons, J. T., and Horwitz, A. R. (2003) *Science* **302,** 1704–1709
10. Burridge, K., and Chrzanowska-Wodnicka, M. (1996) *Annu. Rev. Cell Dev. Biol.* **12,** 463–518
11. Huttenlocher, A., Ginsberg, M. H., and Horwitz, A. F. (1996) *J. Cell Biol.* **134,** 1551–1562
12. Chrzanowska-Wodnicka, M., and Burridge, K. (1996) *J. Cell Biol.* **133,** 1403–1415
13. Zaidel-Bar, R., Ballestrem, C., Kam, Z., and Geiger, B. (2003) *J. Cell Sci.* **116,** 4605–4613
14. Zamir, E., Katz, M., Posen, Y., Erez, N., Yamada, K. M., Katz, B. Z., Lin, S., Lin, D. C., Bershadsky, A., Kam, Z., and Geiger, B. (2000) *Nat. Cell Biol.* **2,** 191–196
15. Peters, D. J., Knecht, D. A., Loomis, W. F., De Lozanne, A., Spudich, J., and Van Haastert, P. J. (1988) *Dev. Biol.* **128,** 158–163
16. Young, P. E., Richman, A. M., Ketchum, A. S., and Kiehart, D. P. (1993) *Genes Dev.* **7,** 29–41
17. Edwards, K., and Kiehart, D. (1996) *Development* **122,** 1499–1511
18. Wheatley, S., Kulkarni, S., and Karess, R. (1995) *Development* **121,** 1937–1946
19. Golomb, E., Ma, X., Jana, S. S., Preston, Y. A., Kawamoto, S., Shoham, N. G., Goldin, E., Conti, M. A., Sellers, J. R., and Adelstein, R. S. (2004) *J. Biol. Chem.* **279,** 2800–2808
20. Simons, M., Wang, M., McBride, O. W., Kawamoto, S., Yamakawa, K., Gdula, D., Adelstein, R. S., and Weir, L. (1991) *Circ. Res.* **69,** 530–539
21. Amano, M., Ito, M., Kimura, K., Fukata, Y., Chihara, K., Nakano, T., Matsuura, Y., and Kaibuchi, K. (1996) *J. Biol. Chem.* **271,** 20246–20249
22. Kimura, K., Ito, M., Amano, M., Chihara, K., Fukata, Y., Nakafuku, M., Yamamori, B., Feng, J., Nakano, T., Okawa, K., Iwamatsu, A., and Kaibuchi, K. (1996) *Science* **273,** 245–248
23. Totsukawa, G., Wu, Y., Sasaki, Y., Hartshorne, D. J., Yamakita, Y., Yamashiro, S., and Matsumura, F. (2004) *J. Cell Biol.* **164,** 427–439
24. Worthylake, R. A., and Burridge, K. (2003) *J. Biol. Chem.* **278,** 13578–13584
25. Eddy, R. J., Pierini, L. M., Matsumura, F., and Maxfield, F. R. (2000) *J. Cell Sci.* **113,** 1287–1298
26. Somlyo, A. V., Bradshaw, D., Ramos, S., Murphy, C., Myers, C. E., and Somlyo, A. P. (2000) *Biochem. Biophys. Res. Commun.* **269,** 652–659
27. Somlyo, A. V., Phelps, C., Dipierro, C., Eto, M., Read, P., Barrett, M., Gibson, J. J., Burnitz, M. C., Myers, C., and Somlyo, A. P. (2003) *FASEB J.* **17,** 223–234
28. Nobes, C. D., and Hall, A. (1999) *J. Cell Biol.* **144,** 1235–1244
29. Arthur, W. T., and Burridge, K. (2001) *Mol. Biol. Cell* **12,** 2711–2720
30. Rottner, K., Hall, A., and Small, J. V. (1999) *Curr. Biol.* **9,** 640–648
31. Cox, E. A., Sastry, S. K., and Huttenlocher, A. (2001) *Mol. Biol. Cell* **12,** 265–277
32. Nobes, C. D., and Hall, A. (1995) *Cell* **81,** 53–62
33. Kelley, C. A., Sellers, J. R., Gard, D. L., Bui, D., Adelstein, R. S., and Baines, I. C. (1996) *J. Cell Biol.* **134,** 675–687
34. Rochlin, M. W., Itoh, K., Adelstein, R. S., and Bridgman, P. C. (1995) *J. Cell Sci.* **108,** 3661–3670
35. Maupin, P., Phillips, C. L., Adelstein, R. S., and Pollard, T. D. (1994) *J. Cell Sci.* **107,** 3077–3090
36. Kolega, J. (1998) *J. Cell Sci.* **111,** 2085–2095
37. Kolega, J. (2003) *Mol. Biol. Cell* **14,** 4745–4757
38. Meigs, T. E., Juneja, J., DeMarco, C. T., Stemmle, L. N., Kaplan, D. D., and Casey, P. J. (2005) *J. Biol. Chem.* **280,** 18049–18055
39. Majumdar, M., Seasholtz, T. M., Buckmaster, C., Toksoz, D., and Brown, J. H. (1999) *J. Biol. Chem.* **274,** 26815–26821
40. Matsumura, F., Ono, S., Yamakita, Y., Totsukawa, G., and Yamashiro, S. (1998) *J. Cell Biol.* **140,** 119–129
41. Tan, J. L., Ravid, S., and Spudich, J. A. (1992) *Annu. Rev. Biochem.* **61,** 721–759
42. Gallagher, P. J., Herring, B. P., Griffin, S. A., and Stull, J. T. (1991) *J. Biol. Chem.* **266,** 23936–23944
43. Tuazon, P. T., and Traugh, J. A. (1984) *J. Biol. Chem.* **259,** 541–546
44. Murata-Hori, M., Suizu, F., Iwasaki, T., Kikuchi, A., and Hosoya, H. (1999) *FEBS Lett.* **451,** 81–84
45. Feng, J., Ito, M., Kureishi, Y., Ichikawa, K., Amano, M., Isaka, N., Okawa, K., Iwamatsu, A., Kaibuchi, K., Hartshorne, D. J., and Nakano, T. (1999) *J. Biol. Chem.* **274,** 3744–3752
46. Murakami, N., Chauhan, V. P., and Elzinga, M. (1998) *Biochemistry* **37,** 1989–2003
47. Riento, K., and Ridley, A. J. (2003) *Nat. Rev. Mol. Cell Biol.* **4,** 446–456
48. Pollard, T. D., and Borisy, G. G. (2003) *Cell* **112,** 453–465
49. Svitkina, T. M., and Borisy, G. G. (1999) *J. Cell Biol.* **145,** 1009–1026
50. Kaverina, I., Krylyshkina, O., and Small, J. V. (2002) *Int. J. Biochem. Cell Biol.* **34,** 746–761
51. Webb, D. J., Parsons, J. T., and Horwitz, A. F. (2002) *Nat. Cell Biol.* **4,** 97–100
52. Smilenov, L. B., Mikhailov, A., Pelham, R. J., Marcantonio, E. E., and Gundersen, G. G. (1999) *Science* **286,** 1172–1174
53. Burridge, K., and Bray, D. (1975) *J. Mol. Biol.* **99,** 1–14
54. Siess, W. (1989) *Physiol. Rev.* **69,** 58–178
55. Straussman, R., Even, L., and Ravid, S. (2001) *J. Cell Sci.* **114,** 3047–3057
56. Rosenberg, M., and Ravid, S. (2006) *Mol. Biol. Cell.* **17,** 1364–1374